

Study of structural and magnetoelectric properties of $1-x(\text{Ba}_{0.96}\text{Ca}_{0.04}\text{TiO}_3)-x(\text{ZnFe}_2\text{O}_4)$ ceramic composites

Madan Lal¹ · Mamta Shandilya¹ · Ajith S. Kumar² · Radheshyam Rai^{1,4}  · Swapna S. Nair² · Ratnakar Palai³

Received: 31 May 2017 / Accepted: 20 September 2017 / Published online: 27 September 2017
© Springer Science+Business Media, LLC 2017

Abstract Multiferroic ceramic composites of $(1-x)\text{Ba}_{0.96}\text{Ca}_{0.04}\text{TiO}_3-x\text{ZnFe}_2\text{O}_4$ (BCT-ZF) were prepared from ferroelectric (FE) barium calcium titanate (BCT) and ferromagnetic (FM) zinc ferrite (ZF) by using the solid state reaction method with different mol% fractions of x ($x=0.1$ and 0.2). The preliminary structural studies carried out by X-ray diffraction at room temperature reveals that the samples have a tetragonal structure along with the cubic spinel ferrite phase. Raman spectra of the composites also confirm the existence of BCT phase and ZF phase. The room temperature ferroelectric polarization measurements as a function of magnetic field show the existence strong magnetoelectric coupling of 10.85 (mV/(cm.Oe)).

1 Introduction

In the twenty-first century, researchers are aiming to discover such materials, whose magnetic and electronic functionality can be controlled by magnetic and electric stimuli in a single phase for novel magnetoelectric devices [1–11] Magnetoelectric (ME) multiferroic materials are the best materials for this novel multifunctional applications. BiFeO_3

(ferroelectric up to ~ 830 °C and antiferromagnetic up to ~ 370 °C) is one the rarest single phase room temperature multiferroic materials with many interesting physical phenomena. However, high leakage current of BiFeO_3 (BFO) and weak magnetoelectric coupling in limits its applications. A strong ME coupling is an important requirement for practical applications. In order to enhance the ME coupling, we synthesized an artificial multiferroics by combining a good ferroelectric and a ferromagnetic phases. The ferrite phase should be highly magnetostrictive possessing high resistivity state which is possible in ZF nanostructure [12], another phase should be highly piezoelectric which is BCT [13]. Such ME materials have a wide range of applications such as chip sensors, multistate memories, actuators and in bio-medical field [14, 15]. The ME effect in composite materials is the result of the interaction between the two-phases (*i.e.* magnetoelectric and ferroelectric): magnetic field induces the structural distortion in the magnetic phase and the applied electric field produces the distortion in ferroelectric phase [16–18]. The ME coupling appeared in materials due to mechanical deformations in the magnetostrictive phase in applied magnetic field δH . Due to the piezoelectric effect, the strains transferred to the piezoelectric phase producing an induced electric field δE in the material. ME voltage coefficient $\alpha E = \delta E / \delta H$ characterizes the ME effect [19, 20].

Lead-free ceramics like BaTiO_3 (BT), $\text{Bi}_{0.5}\text{K}_{0.5}\text{TiO}_3$ (BKT), $\text{K}_{0.5}\text{Na}_{0.5}\text{NbO}_3$, $\text{Bi}_{0.5}\text{Na}_{0.5}\text{TiO}_3$ (BNT). have gained much attention due to their various properties like high dielectric constant [21], high piezoelectricity [22], good mechanical strength [23] and eco-friendly behavior [24–26]. At higher temperature, BCT is cubic (paraelectric), but on cooling it becomes tetragonal (ferroelectric) below Curie temperature of 410 K [27], orthorhombic below 290 K and rhombohedral below 190 K. In 2014 Verma et al. [13] has reported that polycrystalline BT with tetragonal

✉ Radheshyam Rai
rshyam1273@gmail.com

¹ School of Physics and Materials Science, Shoolini University, Solan, H.P 173229, India

² Department of Physics, Central University of Kerala, Kasaragod 671314, India

³ Department of Physics, University of Puerto Rico, San Juan, PR 00936, USA

⁴ Present Address: Department of Physics, Eternal University, Baru Sahib, Sirmour, HP 173101, India

nanostructure has boost polarization due to its twin structure, the stress that resides near the grain boundary can be easily controlled by (i) depolarization field and (ii) long-range interaction.

In bulk form Zinc ferrite ($ZnFe_2O_4$) exhibits normal spinel structure having all Zn^{2+} on A-site and Fe^{3+} on B-site respectively. Due to occupancy of cations on A-site and B-site, these spinel type ferrites show different magnetic behavior. The fact is that the magnetic behavior can be tuned symmetrically by changing the identity or partial substitution of Zn^{2+} cation while maintaining the basic crystal structure. Zn ferrite is paramagnet in bulk at room temperature whereas at nano-scale it shows superparamagnetic behavior [12, 28]. The change in magnetic behavior is due to a cationic distribution, in which Fe^{3+} ions move to tetrahedral sites, and consequently, Zn^{2+} migrates to octahedral sites, which alters the long- and short-range magnetic interactions of A and B sites [29, 30]. In this work, we are presenting the structural, ferroelectric, and magnetoelectric properties of typical perovskite/ferrite composite $((1-x)(Ba_{0.96}Ca_{0.04}TiO_3)-x(ZnFe_2O_4))$ for $x = 0.10$, and 0.20 ceramic composites.

2 Experimental details

Magneto electric composite $(1-x)(Ba_{0.96}Ca_{0.04}TiO_3)-x(ZnFe_2O_4)$ (where $x = 0.10$ and 0.20) consists of two individual phases, one ferroelectric and other ferromagnetic. Zinc ferrite ($ZnFe_2O_4$) was chosen as a ferromagnetic phase and barium titanate ($BaCaTiO_3$) as a ferroelectric phase were prepared by solid state reaction method. The ferrite phase ($ZnFe_2O_4$) was prepared by

using the pure oxides ZnO (99% Merck, India), and Fe_2O_3 (98% Merck, India). The ferroelectric phase was prepared by using the pure oxides $BaCO_3$ (99% Merck, India), $CaCO_3$ (99% Merck, India) and TiO_2 as precursors. Stoichiometric amounts of these oxides were weighed and mixed continuously using agate and pestle in ethanol medium for 4–5 h. Then all the samples were calcined at $900\text{ }^\circ\text{C}$ for 6 h. The fine powder was grind and pressed into green cylindrical pellets using a hydraulic press with a pressure of 50 MPa. These green pellets were sintered at $950\text{ }^\circ\text{C}$ for 3 h. for densification. The formation and superiority of compounds were verified with X-ray diffraction (XRD) technique. X-ray powder diffractometer (Rigaku Miniflex 600, Japan) with $CuK\alpha$ radiation ($\lambda = 1.5405\text{ \AA}$) in an extensive range of Bragg angles 2θ ($20^\circ \leq 2\theta \leq 60^\circ$) at a scanning rate of 2° min^{-1} was used to study the XRD patterns of the compounds at room temperature using. A Jovin Yvon T64000 micro-Raman microprobe system with Ar ion laser $\lambda = 514.5\text{ nm}$ in back-scattering geometry was used for Raman scattering.

Polarization–Electric field (PE) loops tracer (Marine India) was used to study the PE loop at different applied magnetic fields and a DC electromagnet which can go up to 3 kOe. Magnetoelectric coupling measurements were done with an automated system (Marine India).

3 Result and discussion

3.1 Structural studies

Figure 1a shows the XRD patterns of $(1-x)(Ba_{0.96}Ca_{0.04}TiO_3)-x(ZnFe_2O_4)$ powder at room temperature. The pattern confirms the coexistence of two phases

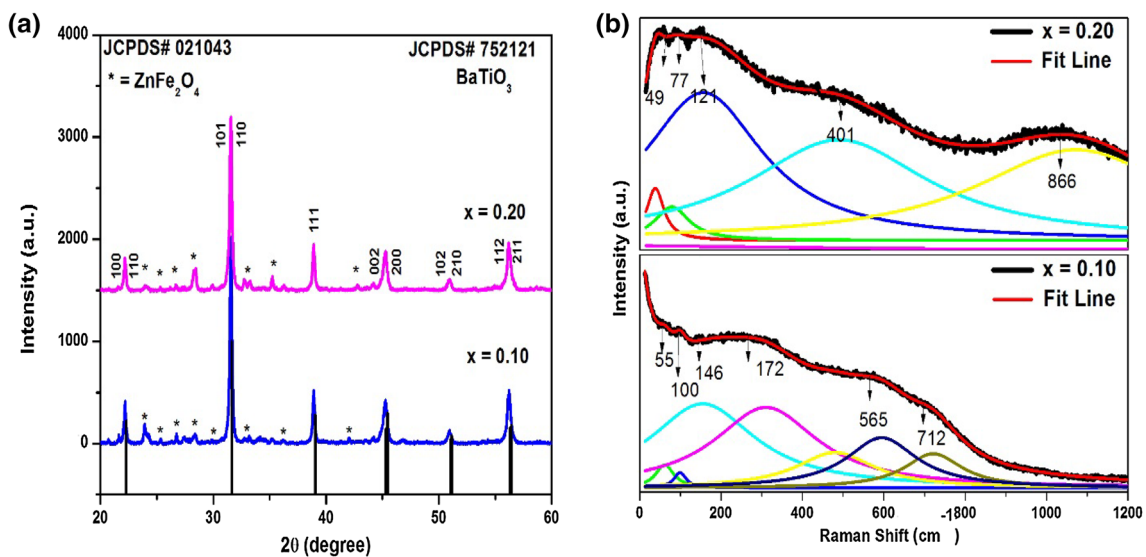


Fig. 1 a X-Ray diffraction patterns, b Raman spectra of BCT–ZF (where $x = 0.10$ and 0.20) powders

namely perovskite and spinel corresponding to BCT and ZF, respectively. The polycrystalline BCT of tetragonal phase at diffraction angle $2\theta = 22.15, 31.57, 38.89, 45.25, 50.93$ and 56.19° are corresponds to (100/110), (101/110), (111), (002/200), (102/201) and (112/211) respectively, (matched with JCPDS#752121 data). A secondary phase of (ZnFe_2O_4) was observed (shown as * in Fig. 1a) in $(1-x)$ ($\text{Ba}_{0.96}\text{Ca}_{0.04}\text{TiO}_3$)– $x(\text{ZnFe}_2\text{O}_4)$ sample and was certified that ZnFe_2O_4 have cubic spinel phase (JCPDS#021043). The calculated average crystalline size by using Debye–Scherrer formula [31] is ~ 32 and 22 nm for BCT–ZF ceramics ($x = 0.10$ and 0.20) respectively.

Figure 1b shows Raman spectra of $(1-x)$ $\text{Ba}_{0.96}\text{Ca}_{0.04}\text{TiO}_3$ – $x(\text{ZnFe}_2\text{O}_4)$ (BCT–ZF) ($x = 0.10$ and 0.20). The asymmetric and broad peaks at 100 cm^{-1} [$A_1(\text{TO}_1)$], 120 – 180 cm^{-1} [$A_1(\text{TO}_2)$], 717 cm^{-1} [$A_1(\text{LO})$]/ $E(\text{TO})$], symmetric intense peak at 515 cm^{-1} [$A_1(\text{TO}_3)$]/ $E(\text{TO})$] correspond to the BaTiO_3 tetragonal phase [32]. The Raman bands at 100 – 180 , 268 – 305 , and 710 – 716 cm^{-1} are apparent for the tetragonal phase in all the BCT–ZF samples [33]. For $x = 0.10$ peak shift towards lower wave number $\sim 55 \pm 5\text{ cm}^{-1}$ and $\sim 100 \pm 1\text{ cm}^{-1}$. The composition $0.80(\text{Ba}_{0.96}\text{Ca}_{0.04}\text{TiO}_3)$ – $0.20(\text{ZnFe}_2\text{O}_4)$, notice the narrowing of the bands and intensification of the scattering at lower energy $\sim 49 \pm 1$ and $\sim 77 \pm 2\text{ cm}^{-1}$. It establishes evidence that ZF phase coexists with BCT phase. Cubic spinel zinc ferrite (ZF) has space group $O_h^7 (Fd3m)$ with eight formula units per unit cell [34].

3.2 Ferroelectric properties

The ferroelectric behavior of BCT–ZF composites is shown in (Fig. 2a–f). In present magnetodielectric composite system, percentage dielectric phase has the significant effect in the polarization response. Polarization in the material generally comes from the dielectric phase. It was observed that the responses of PE loop of the present BCT: ferrite composites deviated from the ideal ferroelectric loop. The particular ferrite based composites appear in oval shape indicating lossy capacitor phenomena due to field discharge by conductive ferrite phase [35, 36]. However, all ferrite based magnetoelectric composites show near ferroelectric behavior due to maximum dielectric phase in the composite, also it can be true that it has less loss compared with ferrite composites, which can be said by the area enclosed by PE loop.

Initially, remnant polarization (P_r) decreases with the DC bias field up to 1 kOe and then started to increase. The initial decrease is due to ME coupling between the ferroic orders in the sample mediated via strain (Fig. 2g). Around 1 kOe , the P_r value reaches the lowest value, this because of magnetostriction reaches to its maximum value (as shown in Fig. 4a). Since the magnetostriction coefficient is low at the higher field because of which the ME coupling contribution

towards the net polarization is low. As the applied magnetic field increases, the magnetoresistance effects become dominant [37]. This increase in magnetoresistance may results in the decrease of leakage current through the ferroelectric phase, which enhances the polarization beyond 1 kOe .

The room temperature capacitance vs. frequency at different magnetic fields is shown in (Fig. 3a and b). In these measurements, the magnetic field was applied in a direction perpendicular to the direction of measurement of capacitance. The overall dielectric behavior is of Maxwell–Wagner type [38, 39]. At low frequencies, the charge carriers get accumulated at the grain boundaries resulting in a high capacitance. The capacitance decrease almost exponentially with the increase in frequency. This is due to the fact that the charge carriers in the dielectric medium could not follow the high frequency of the alternating field. The dispersion is shown in [(Fig. 3a and b (inset))] being due to the phenomenon called the magnetocapacitance effect.

3.3 Magnetoelectric coupling measurements

The origin of ME coupling of BCT–ZF composite is the coupling of FE and FM degrees of freedom due to the influence of FE on the exchange coupling constant via screening of the intra and inter-grain coulomb's interaction. Therefore, a possible mechanism for ME coupling of this FE/FM (BCT–ZF) interface is based on screening effects [40]. The spin-polarized charge density formed in the FM in the vicinity of the FM/FE interface [41] acts with a torque on the magnetic moments in the FM, resulting in a non-collinear magnetic ordering [42]. Hence, electric polarization emerges that couples the FM to the FE part. Additionally, the FE polarization (and electric field) stems actually from the FE surface which triggers the spin spiral in FM. The latter carries a spin current with an associated Aharonov–Casher effect and/or Dzyaloshinskii–Moriya (DM) interaction [43]. In this sense the ME coupling caused by an emergent inverse DM interaction at MF interfaces [13, 17]. The variation of α_E with H_{dc} at ac modulating field of 50 Oe and ac frequency of 50 Hz along the longitudinal mode shows in Fig. 4a. ZF is a negative magnetostrictive material, by which ZF particles contract along the direction of application of a magnetic field, resulting in a polarization of the BCT particles in a direction between the particles. The ME coupling coefficient increases initially with the applied DC magnetic field reach a maximum value and then decreases. Similar trends are already reported by various groups [44–46]. The initial increase in ME coupling coefficient is due to increase in magnetostriction of ferrite with applied DC field. The magnetostriction reaches a maximum value at a particular magnetic field beyond which the magnetostriction produces a nearly constant change in polarization. As a

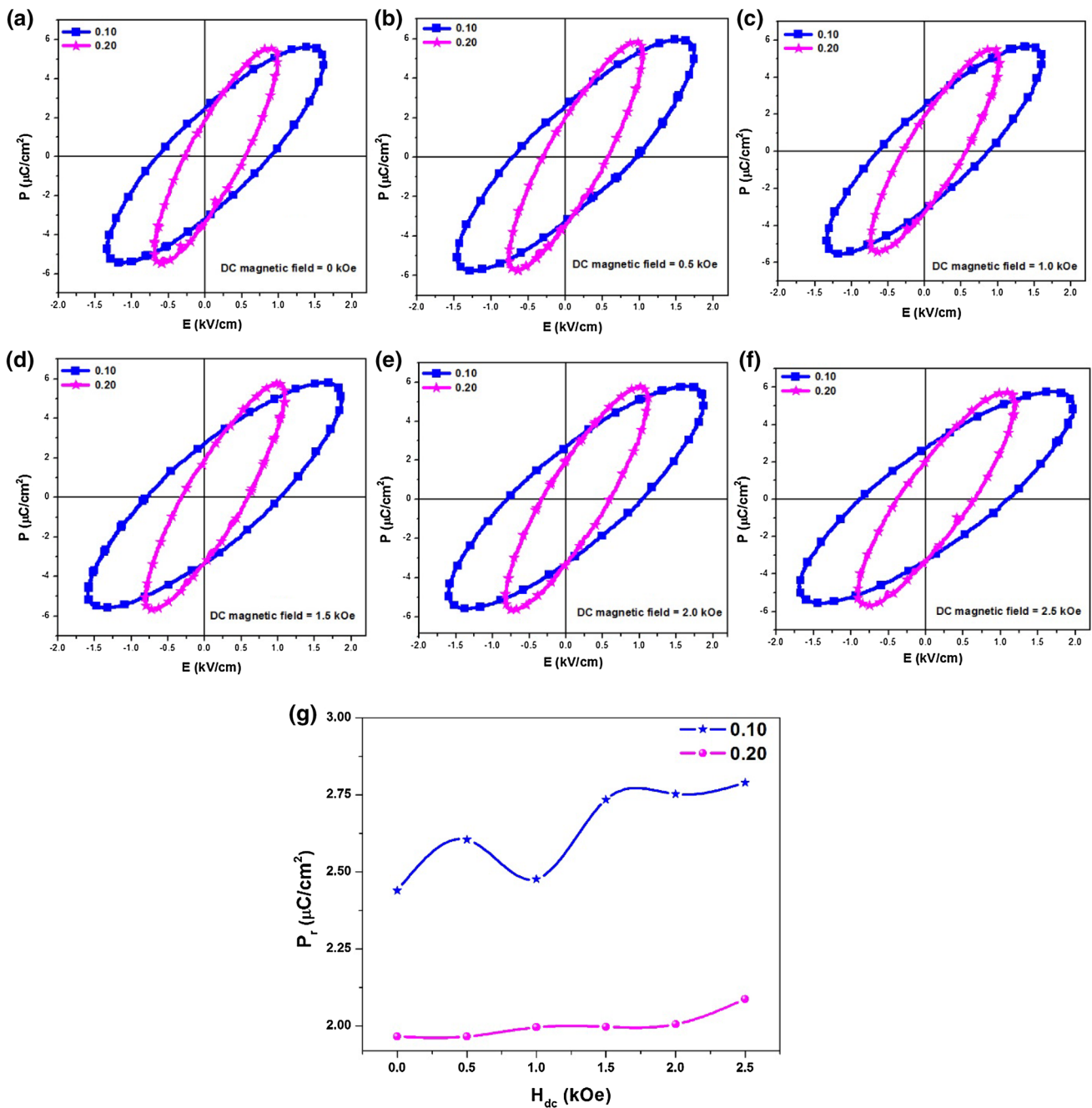


Fig. 2 a–f Polarization–Electric field loop of BCT–ZF (where $x=0.10$ and 0.20) ceramics at different DC bias fields. Electric polarization can be easily tuned by applying DC magnetic fields and **g** Variation of remnant polarization (P_r) with applied magnetic field

result, the ME coupling coefficient decreases with further increase in magnetic field. ME measurement shows maximum coupling coefficient of 10.85 and 6.85 $\text{mV}/(\text{cm Oe})$ for $x=0.10$ and 0.20 , respectively at a DC biasing field of 1.0 kOe. Corral-Flores et al. reported an MECC value of 1.48 $\text{mV}/(\text{cm.Oe})$ for BTO–CFO [47]. The observed α_E in our samples is ~ 10 times larger than the reported values

of BTO–CFO composites. This may be due to the presence of the leakage currents, which is evident from the round shaped ferroelectric hysteresis loop. Figure 4b shows that the induced ME voltage has a linear dependence on the AC magnetic field. These results point to the fact that the ME composite developed in the study has a very good response to even a small variation in AC magnetic field.

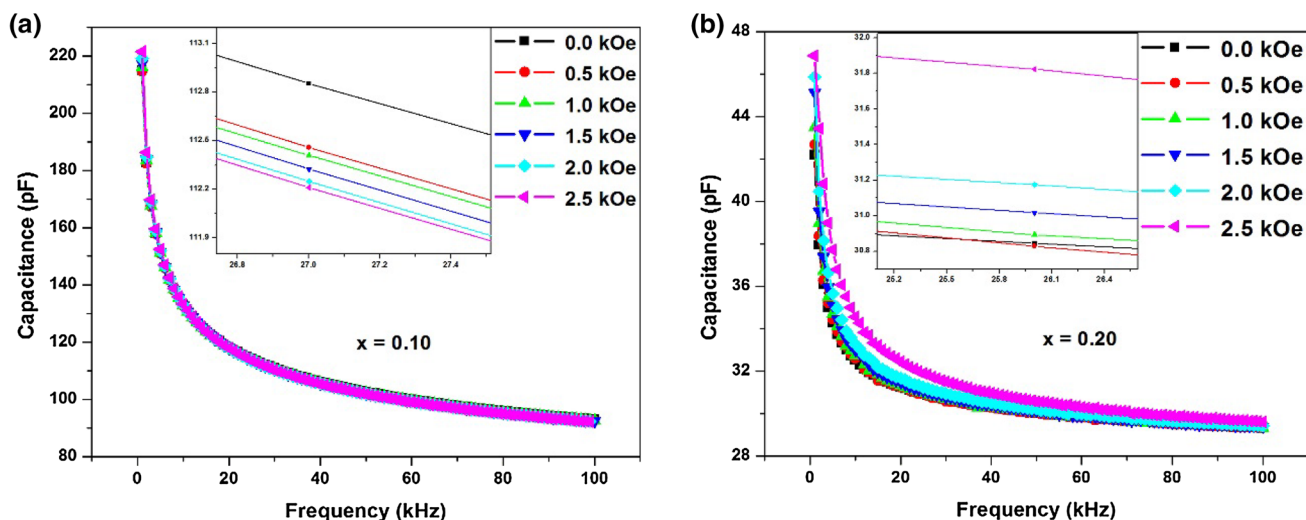


Fig. 3 a–b Capacitance versus frequency curves measured at different applied DC magnetic fields for BCT–ZF ($x=0.10$ and 0.20) ceramics

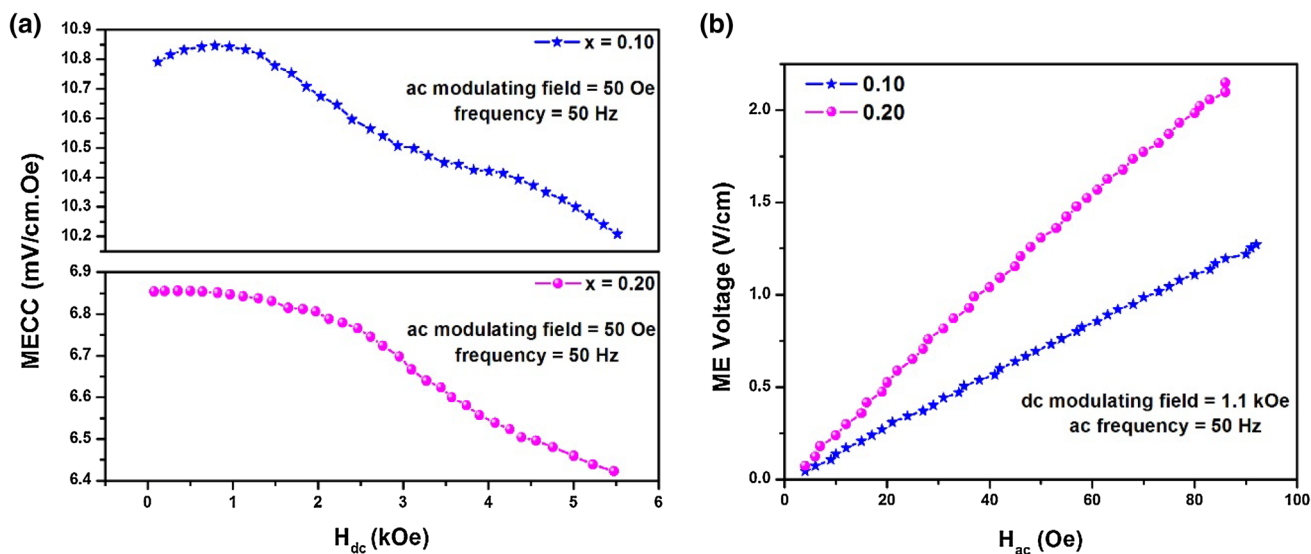


Fig. 4 a DC field dependence of MECC and b ME voltage as a function of applied AC magnetic field of BCT–ZF (where $x=0.10$ and 0.20) ceramics

4 Conclusion

Composite Ceramics of $(1-x)$ $(\text{Ba}_{0.96}\text{Ca}_{0.04}\text{TiO}_3)$ – $x(\text{ZnFe}_2\text{O}_4)$ with two phases were prepared by the solid-state reaction method. The capacitance and the polarization of the sample are found to be magnetically tunable. The composites have shown MECC of 10.85 and 6.85 mV/(cm Oe), and are highly sensitive to the AC magnetic field. These properties suggested the suitability of these composites be used exploited in magnetic-field-controlled ferroelectric capacitors namely Magneto varactors implemented in electronic oscillators, where the oscillation frequency is tuned by a dc magnetic field remotely

(via the change of capacitance) in contrast to conventional voltage-controlled oscillators.

Acknowledgements Authors are grateful to the Defence Research and Development Organization (DRDO), Govt. of India, for financial support under the research project ERIP/ER/1303129/M/01/1564. The work at UPR is support by National Science Foundation (NSF DMR-1410869).

References

1. H. Schmid, Multi-ferroic magnetoelectrics. *Ferroelectrics* **162**(1), 317–338 (1994)

2. P. Fischer et al., Temperature dependence of the crystal and magnetic structures of BiFeO₃. *J. Phys. C* **13**(10), 1931 (1980)
3. G.A. Smolenskii, I.E. Chupis, Ferroelectromagnets. *Soviet Phys. Uspekhi* **25**(7), 475 (1982)
4. J. Wang et al., Epitaxial BiFeO₃ multiferroic thin film heterostructures. *Science* **299**(5613), 1719 (2003)
5. Y. Tokura, Multiferroics as quantum electromagnets. *Science* **312**(5779), 1481 (2006)
6. J.F. Scott, Data storage: multiferroic memories. *Nat Mater.* **6**(4), 256–257 (2007)
7. R. Palai et al., β phase and γ – β metal-insulator transition in multiferroic Bi Fe O₃. *Phys. Rev. B* **77**(1), 014110 (2008)
8. R. Palai, J.F. Scott, R.S. Katiyar, Phonon spectroscopy near phase transition temperatures in multiferroic BiFeO₃ epitaxial thin films. *Phys. Rev. B* **81**(2), 024115 (2010)
9. S.Y. Yang et al., Metalorganic chemical vapor deposition of lead-free ferroelectric BiFeO₃ films for memory applications. *Appl. Phys. Lett.* **87**(10), 102903 (2005)
10. G. Catalan, J.F. Scott, Physics and applications of bismuth ferrite. *Adv. Mater.* **21**(24), 2463–2485 (2009)
11. S.V. Kalinin, Multiferroics: Making a point of control. *Nat. Phys.*, **13**, 115–116 (2017)
12. S. Nakashima et al., First-principles XANES simulations of spinel zinc ferrite with a disordered cation distribution. *Phys. Rev. B* **75**(17), 174443 (2007)
13. K.C. Verma, S. Tripathi, R. Kotnala, Magneto-electric/dielectric and fluorescence effects in multiferroic x BaTiO₃–(1–x) ZnFe₂O₄ nanostructures. *RSC Adv.* **4**(104), 60234–60242 (2014)
14. E.V. Ramana et al., Effect of Fe-doping on the structure and magnetoelectric properties of (Ba 0.85 Ca 0.15)(Ti 0.9 Zr 0.1) O₃ synthesized by a chemical route. *J. Mater. Chem. C* **4**(5), 1066–1079 (2016)
15. M. Bichurin et al., Magnetolectric effect in layered structures of amorphous ferromagnetic alloy and gallium arsenide. *J. Magn. Magn. Mater.* **424**, 115–117 (2017)
16. A. Sukhov et al., Magnetolectric coupling in a ferroelectric/ferromagnetic chain revealed by ferromagnetic resonance. *J. Appl. Phys.* **113**(1), 013908 (2013)
17. C.-L. Jia et al., Mechanism of interfacial magnetolectric coupling in composite multiferroics. *Phys. Rev. B* **90**(5), 054423 (2014)
18. R. Rai et al., Dielectric and magnetic studies of (NKNLS) 1–x–(NZFO) x multiferroic composites. *J. Alloys Compd.* **614**, 277–282 (2014)
19. J. Ma et al., Recent progress in multiferroic magnetolectric composites: from bulk to thin films. *Adv. Mater.* **23**(9), 1062–1087 (2011)
20. C.-W. Nan et al., Multiferroic magnetolectric composites: historical perspective, status, and future directions. *J. Appl. Phys.* **103**(3), 031101 (2008)
21. P. Kumaria et al., State-of-the-art of lead free ferroelectrics: a critical review. *Adv. Mater. Lett.* **6**(6), 453–484 (2015)
22. W. Liu, X. Ren, Large piezoelectric effect in Pb-free ceramics. *Phys. Rev. Lett.* **103**(25), 257602 (2009)
23. T. Tou et al., Properties of (Bi_{0.5}Na_{0.5}) T 3 3 0 5 N 0 1 N₂O₃ lead-free piezoelectric ceramics and its application to ultrasonic cleaner. *Jpn. J. Appl. Phys.* **48**(7S), 07GM03 (2009)
24. M. Lal et al., Structural, Dielectric and Impedance Studies of KNN–BKT Ceramics. *Am. J. Mater. Sci.* **7**(2), 25–34 (2017)
25. A. Singh, R. Chatterjee, Structural and electrical properties of BKT rich Bi_{0.5}K_{0.5}TiO₃–K_{0.5}Na_{0.5}NbO₃ system. *AIP Adv.* **3**(3), 032129 (2013)
26. H.F. Kay, P. Vousden, XCV. Symmetry changes in barium titanate at low temperatures and their relation to its ferroelectric properties. London, Edinburgh, and Dublin Philos. Mag. J. Sci. **40**(309), 1019–1040 (1949)
27. A. Bratkovsky, A. Levanyuk, Smearing of phase transition due to a surface effect or a bulk inhomogeneity in ferroelectric nanostructures. *Physical Rev. Lett.* **94**(10), 107601 (2005)
28. E.J. Choi, Y. Ahn, E.J. Hahn, Size dependence of the magnetic properties in superparamagnetic zinc-ferrite nanoparticles. *J. Kor. Phys. Soc.* **53**(4), 2090–2094 (2008)
29. J. Hocheplied, P. Bonville, M. Pileni, Nonstoichiometric zinc ferrite nanocrystals: syntheses and unusual magnetic properties. *J. Phys. Chem. B* **104**(5), 905–912 (2000)
30. S. Stewart et al., Cationic exchange in nanosized Zn Fe₂O₄ spinel revealed by experimental and simulated near-edge absorption structure. *Phys. Rev. B* **75**(7), 073408 (2007)
31. S. Kumar, N. Ahlawat, N. Ahlawat, Microwave sintering time optimization to boost structural and electrical properties in BaTiO₃ ceramics. *J. Integr. Sci. Technol.* **4**(1), 10–16 (2016)
32. V.S. Puli et al., Structure, dielectric tunability, thermal stability and diffuse phase transition behavior of lead free BZT–BCT ceramic capacitors. *J. Phys. Chem. Solids* **74**(3), 466–475 (2013)
33. J. Pokorný et al., Use of Raman spectroscopy to determine the site occupancy of dopants in BaTiO₃. *J. Appl. Phys.* **109**(11), 114110 (2011)
34. J.P. Singh et al., Micro-Raman investigation of nanosized zinc ferrite: effect of crystallite size and fluence of irradiation. *J. Raman Spectrosc.* **42**(7), 1510–1517 (2011)
35. A. Khamkongkao et al., Frequency-dependent magnetoelectricity of CoFe₂O₄–BaTiO₃ particulate composites. *Trans. Nonferr. Metals Soc. China* **21**(11), 2438–2442 (2011)
36. S. Pachari, *Structure, microstructure and magneto-dielectric properties of barium titanate-ferrite based composites*. (National Institute of Technology Rourkela, Rourkela, 2015)
37. A.S. Kumar et al., Multiferroic and magnetoelectric properties of Ba 0.85Ca 0.15 Zr 0.1 Ti 0.9O₃–CoFe₂O₄ core–shell nanocomposite. *J. Magn. Magn. Mater.* **418**, 294–299 (2016)
38. K.W. Wagner, Zur theorie der unvollkommenen dielektrika. *Ann. Phys.* **345**(5), 817–855 (1913)
39. C. Koops, On the dispersion of resistivity and dielectric constant of some semiconductors at audiofrequencies. *Phys. Rev.* **83**(1), 121 (1951)
40. O. Udalov, N. Chitchekatchev, I. Beloborodov, Coupling of ferroelectricity and ferromagnetism through Coulomb blockade in composite multiferroics. *Phys. Rev. B* **89**(17), 174203 (2014)
41. L. Chotorlishvili et al., Dynamics of localized modes in a composite multiferroic chain. *Phys. Rev. Lett.* **111**(11), 117202 (2013)
42. N. Sedlmayr, V. Dugaev, J. Berakdar, Current-induced interactions of multiple domain walls in magnetic quantum wires. *Phys. Rev. B* **79**(17), 174422 (2009)
43. H. Katsura, N. Nagaosa, A.V. Balatsky, Spin current and magnetolectric effect in noncollinear magnets. *Phys. Rev. Lett.* **95**(5), 057205 (2005)
44. S.S. Nair et al., Lead free heterogeneous multilayers with giant magneto electric coupling for microelectronics/microelectromechanical systems applications. *J. Appl. Phys.* **114**(6), 064309 (2013)
45. H. Greve et al., Giant magnetolectric coefficients in (Fe 90 Co 10) 78 Si 12 B 10–AlN thin film composites. *Appl. Phys. Lett.* **96**(18), 182501 (2010)
46. C.-W. Nan et al., Large magnetolectric response in multiferroic polymer-based composites. *Phys. Rev. B* **71**(1), 014102 (2005)
47. V. Corral-Flores et al., Enhanced magnetolectric effect in core-shell particulate composites. *J. Appl. Phys.* **99**(8), 08J503 (2006)